
Article:
Qu, H. orcid.org/0000-0001-7136-4440, Zhu, Z.Q. orcid.org/0000-0001-7175-3307, Matsuura, T. et al. (8 more authors) (2021) Comparative study of dual PM vernier machines. World Electric Vehicle Journal, 12 (1). 12.

https://doi.org/10.3390/wevj12010012

World Electric Vehicle Journal

MDPI

Article

Comparative Study of Dual PM Vernier Machines

Huan Qu [1], Zi Qiang Zhu [1,*], Toru Matsuura [2], Dusan Ivanovic [2], Takashi Kato [2], Kensuke Sasaki [2], Jim Greenough [2], Bob Bateman [2], David A. Stone [1], Martin P. Foster [1] and Javier Riedemann [1]

[1] Department of Electronic and Electrical Engineering, University of Sheffield, Mappin Street, Sheffield S1 3JD, UK; hqu2@sheffield.ac.uk (H.Q.); d.a.stone@sheffield.ac.uk (D.A.S.); m.p.foster@sheffield.ac.uk (M.P.F.); j.riedemann@sheffield.ac.uk (J.R.)

[2] Research & Advanced Engineering, Nissan Technical Centre Europe, Cranfield Technology Park, Cranfield MK43 0DB, UK; t-matsuura@mail.nissan.co.jp (T.M.); dusan.ivanovic@ntc-europe.co.uk (D.I.); katou-t@mail.nissan.co.jp (T.K.); kensuke-sasaki@mail.nissan.co.jp (K.S.); jim.greenough-extern@ntc-europe.co.uk (J.G.); bob.bateman@ntc-europe.co.uk (B.B.)

* Correspondence: z.q.zhu@sheffield.ac.uk; Tel.: +44-(0)114-222-5195

Abstract: In this paper, two types of dual permanent magnet (PM) machines, i.e., stator slot dual-PM (SSDPM) machine and split-tooth dual-PM (STDPM) machine, are investigated and compared. Both machines have consequent pole structure with Halbach array PMs. Their difference lies in the position of stator PM. The SSDPM machine has Halbach array PMs in the stator slots, while the STDPM machine has PMs between the split teeth. Torque characteristics, i.e., average torques and torque ripples, of different slot/pole number combinations of the two machines are compared. The 24 stator slots/20 rotor slots/4 armature pole pair (24S20R4Pa) SSDPM machine with distributed windings and the 24 stator slots/10 rotor slots/4 armature pole pair (12S20R4Pa) STDPM machine with concentrated windings are compared under both open-circuit and on-load conditions. The results show that the SSDPM machine is more competitive by delivering higher torque density and higher power density.

Keywords: dual permanent magnet (PM); electric vehicle (EV); flux modulation; Halbach PM array

Citation: Qu, H.; Zhu, Z.Q.; Matsuura, T.; Ivanovic, D.; Kato, T.; Sasaki, K.; Greenough, J.; Bateman, B.; Stone, D.A.; Foster, M.P.; et al. Comparative Study of Dual PM Vernier Machines. *World Electr. Veh. J.* **2021**, *12*, 12. https://doi.org/10.3390/wevj12010012

Received: 30 December 2020
Accepted: 8 January 2021
Published: 12 January 2021

1. Introduction

Recently, flux modulation (FM) machines have been widely investigated due to their high torque density [1–5]. They can be a strong competitor for interior permanent magnet (IPM) machines.

Research shows that different FM machines, i.e., flux-switching permanent magnet (PM) (FSPM) machines, flux reversal PM (FRPM) machines, doubly salient PM (DSPM) machines, vernier PM (VPM) machines, magnetically geared machines, etc., share the same operation principle, i.e., magnetic gearing effect or flux modulation effect [6–9]. The FM machines can also be categorified by PM positions and stator/rotor numbers: stator PM FM machines that have PMs in the stator [10–14], rotor PM FM machines that have PMs in the rotor [15,16], dual-PM FM machines that have PMs in both the rotor and stator [5,17–22], dual stator/single rotor FM machines that have two stators and one single rotor [4,23–28], dual rotor/single stator FM machines that have two rotors and one stator [1–3,29], triple rotor/dual stator FM machines that have three rotors and two stators [30], etc.

Stator PM FM machines include FSPM machines, FRPM machines, and DSPM machines [10–14]. FSPM machines have better flux-focusing effect than the other two types of machines. Stator PM machines have easier heat management if a forced liquid cooling is employed. This means that the electric loading can be further increased to improve the torque density. Rotor PM FM machines mainly refer to VPM machines, which can produce high torque at low speed, albeit with poor power factor [15,16].

To further enhance the torque density, dual stator/single rotor [4,23–28], dual rotor/single stator [1–3,29], and multi stator/multi rotor [30] PM machines are proposed and

developed, albeit with complex structures. Dual-PM machines can also help to increase the torque density significantly due to torque contribution by both stator PM and rotor PM [5,17–22].

In this paper, two types of dual-PM machines, i.e., stator slot dual-PM (SSDPM) machine and split-tooth dual-PM (STDPM) machine, together with consequent pole rotors, are investigated and compared. On one hand, they can deliver very high torque. More importantly, since there is only one airgap, they have much simpler structures than dual-stator/dual-rotor machines. The working principle, slot/pole number combination, together with comparison of two dual-PM machines, will be discussed. Figure 1 shows the SSDPM machine with 24 stator slots/20 rotor slots/4 armature pole pair (24S20R4Pa) and split-tooth dual-PM (STDPM) machine with (12S20R4Pa).

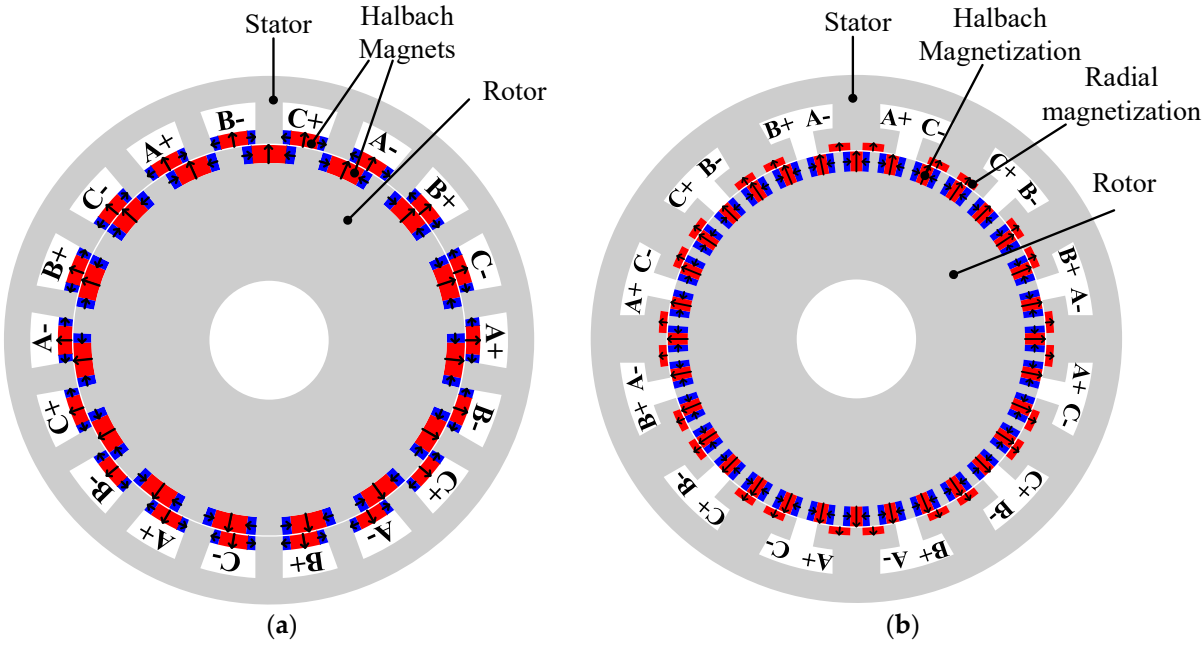

Figure 1. Machine topologies of dual permanent magnet (PM) machines. (**a**) 24S20R4Pa stator slot dual-PM (SSDPM) machine; (**b**) 12S20R4Pa split-tooth dual-PM (STDPM) machine.

2. Machine Topologies and Working Principle

2.1. Machine Topology

In [5], the dual-PM machine employs radially magnetized PMs in both the rotor slots and the stator slots. Article [20] improves the dual-PM machine by replacing the radially magnetized stator PMs with Halbach PMs. In this paper, to further enhance the torque density, dual Halbach PMs are employed in the SSDPM machine, as shown in Figure 1a. Both the rotor PM and stator PM are Halbach PM arrays.

The STDPM machines also employ Halbach PM array in the rotor slots, but with radially magnetized PMs between the split teeth [17].

2.2. Working Principle

For the dual-PM machines, the torque can be attributed to two parts: rotor PM and stator PM. The 12S11R1Pa SSDPM machine and 12S23R1Pa STDPM machine are taken as examples to explain the machine decomposition, as shown in Figures 2 and 3. The key design dimensions are shown in Figure 4. The design details are given in Tables 1 and 2.

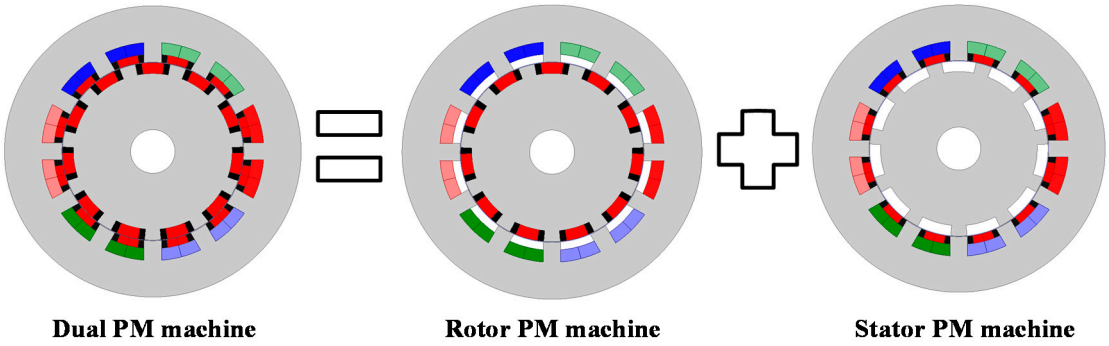

Figure 2. Machine decomposition of 12S11R1Pa SSDPM machine.

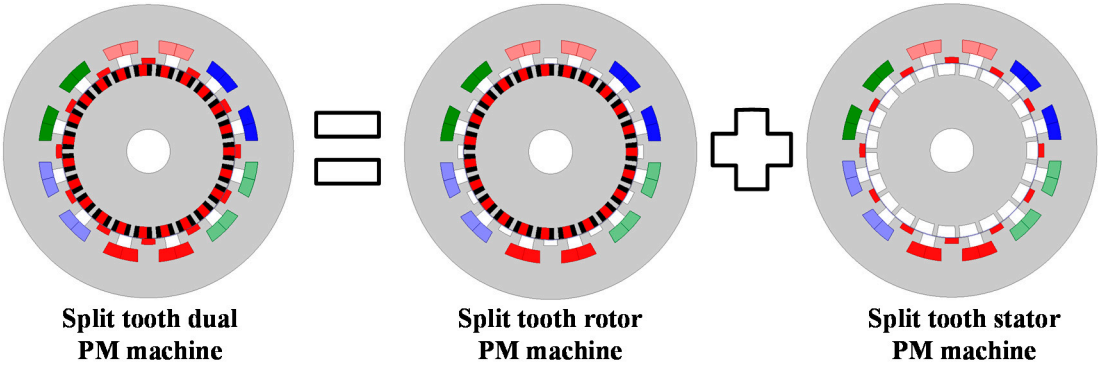

Figure 3. Machine decomposition of 12S23R1Pa STDPM machine.

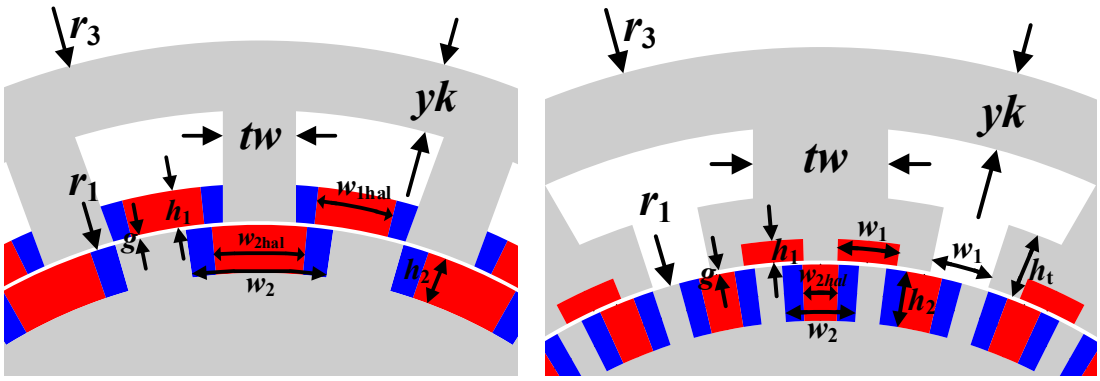

(**a**) SSDPM machine (**b**) STDPM machine

Figure 4. Key design dimensions of dual-PM machines. (**a**) SSDPM machine; (**b**) STDPM machine.

On one hand, when the stator PMs are set as air, they become vernier PM machines and split-tooth vernier PM machines, and the slot/pole number combinations comply with the Equation (1) [31] and Equation (2) [32], respectively.

$$N_r = N_s \pm P_a, \quad (1)$$

$$N_r = nN_s \pm P_a, \quad (2)$$

in which N_s is the stator slot number, N_r is the rotor slot number, P_a is the armature pole pair number, n is the split tooth number which is larger than 1.

On the other hand, when the rotor PMs are set as air, they become flux reversal PM machines, and the slot/pole number combinations also comply with the above-mentioned equations. Hence, the slot/pole number combinations of dual-PM machines comply with

(1) and (2). To calculate the torque decomposition of dual-PM machines, linear material is employed, and the relative permeability is set as 50, considering the overload capability.

Before discussing detailed results, it should be mentioned that the torque, power, iron loss, power factor, back EMF, etc., are all normalized due to confidentiality. As shown in Figure 5, for the 12S11R1Pa SSDPM machine, the rotor PM machine and the stator PM machine produce 0.515 p.u. and 0.335 p.u. torque, respectively. The dual-PM machine delivers 1.7% lower torque than the sum of the rotor PM machine and the stator PM machine. This is mainly due to that the flux leakage increases when the rotor PM and stator PM are working together. Similarly, for the 12S23R1Pa STDPM machine, the dual-PM machine produces 1.5% lower torque than the sum of the corresponding rotor PM machine and stator PM machine, as shown in Figure 6.

Table 1. Parameters of optimized SSDPM machines with different slot/pole number combinations.

Symbol	12S11R 1Pa	12S13R 1Pa	12S10R 2Pa	12S8R 4Pa	12S7R 5Pa	18S17R 1Pa	18S16R 2Pa	18S15R 3Pa	18S14R 4Pa	18S13R 5Pa	24S23R 1Pa	24S22R 2Pa	24S20R 4Pa	24S19R 5Pa	24S16R 8Pa	24S14R 10Pa
r_3 (mm)	100															
l_{stk} (mm)	140															
g (mm)	0.5															
B_r, μ_r	1.3 T, 1.05															
tw (mm)	11.7	8.5	13.5	16	18.2	5.75	9.2	10.3	10.3	10.6	5.0	6.5	6.95	8.4	8.6	9.6
w_2 (deg)	10.4	17.6	26.2	30.3	35.9	13.1	15.4	16.2	18.0	18.3	9.9	9.9	10.5	10.9	12.5	17.5
yk (mm)	25.1	22.3	14.5	9.3	9.4	25.8	13.2	9.9	6.3	6.7	24.6	15.4	9.6	8.1	5.5	5.9
r_1 (mm)	60.9	64.3	67.8	70	65.7	62.1	69.8	73.8	69.0	72.6	64.8	71.5	73.0	74.2	75.9	68.1
h_1 (mm)	5.3	5.2	4.7	4.2	4.9	5.3	4.3	5.3	4.7	4.4	5.1	4.9	4.1	4.5	5.1	4.2
h_2 (mm)	7.4	7.3	7.1	6.7	7.3	7.2	7.0	6.8	7.4	7.3	7.3	7.1	7.1	6.2	7.2	7.4
S_{slot} (mm^2)	208.0	232.3	349.9	436.8	470.6	120.0	231.4	202.8	370.6	303.5	70.4	112.7	192.5	177.8	187.7	260.9
w_{1hal}	0.63	0.58	0.60	0.66	0.4	0.41	0.5	0.64	0.58	0.52	0.39	0.41	0.58	0.53	0.4	0.51
w_{2hal}	0.64	0.62	0.75	0.72	0.78	0.59	0.71	0.65	0.66	0.64	0.60	0.58	0.64	0.7	0.74	0.69
Symbol	**30S29R 1Pa**	**30S28R 2Pa**	**30S26R 4Pa**	**30S25R 5Pa**	**30S23R 7Pa**	**30S22R 8Pa**	**30S20R 10Pa**	**36S35R 1Pa**	**36S34R 2Pa**	**36S33R 3Pa**	**36S32R 4Pa**	**36S31R 5Pa**	**36S30R 6Pa**	**36S29R 7Pa**	**36S28R 8Pa**	**36S26R 10Pa**
tw (mm)	5.2	5.2	7.3	6.9	7.3	7.9	8.1	4.0	4.0	5.0	5.1	6.7	5.2	6.8	6.2	7.3
w_2 (deg)	8.6	8.9	9.5	10.8	10.7	11.4	12.6	7.5	7.3	7.7	7.7	7.7	7.6	7.7	9.0	9.1
yk (mm)	24.8	14.6	8.6	7.7	6.3	5.1	4.3	23.5	15.0	9.9	9.7	7.3	6.2	6.8	5.5	4.8
r_1 (mm)	64.9	74.2	76.3	77.9	73.9	74.2	71.4	67.5	67.5	77.8	75.3	78.1	76.9	78.7	77.4	78.5
h_1 (mm)	5.4	4.0	4.9	3.8	3.8	3.8	3.7	3.8	4.4	5.5	4.7	3.5	3.5	3.5	4.5	3.9
h_2 (mm)	6.9	6.9	6.4	7.4	7.0	6.5	7.1	6.4	6.6	7.1	6.5	7.4	6.0	7.4	6.7	7.1
S_{slot} (mm^2)	44.4	80.3	105.0	114.9	165.9	168.2	197.8	42.0	122.7	64.1	96.1	90.7	129.6	89.8	111.8	101.4
w_{1hal}	0.50	0.42	0.56	0.43	0.41	0.39	0.79	0.31	0.34	0.49	0.33	0.54	0.41	0.58	0.44	0.63
w_{2hal}	0.38	0.57	0.50	0.66	0.55	0.68	0.54	0.41	0.48	0.39	0.40	0.55	0.53	0.50	0.45	0.49

Table 2. Parameters of optimized 6-slot STDPM machines with a different split-tooth number and armature pole pair number.

Symbol	2 Split-Tooth			3 Split-Tooth			4 Split-Tooth		
	6S11R1Pa	**6S10R2Pa**	**6S8R4Pa**	**6S17R1Pa**	**6S16R2Pa**	**6S14R4Pa**	**6S23R1Pa**	**6S22R2Pa**	**6S20R4Pa**
tw (mm)	34.5	34.9	34.1	17.7	37.8	15.5	26.9	34.0	28.8
w_1 (deg)	19.7	19.1	17.3	12.3	12.0	11.4	9.2	7.8	8.9
yk (mm)	22.4	21.0	13.8	25.4	16.1	9.5	25.8	14.9	11.2
h_t (mm)	7.9	7.0	7.3	7.2	7.1	6.1	6.2	8	5.7
so (deg)	19.7	19.1	17.3	12.3	12	11.4	9.2	7.8	8.9
r_1 (mm)	61.5	56.7	61.8	59.9	62.6	75.3	60.4	64.8	73.8
h_1 (mm)	4.2	4.0	4.8	4.4	4.5	4.7	4.4	4.8	4.8
h_2 (mm)	7.7	8.0	7.1	7.5	7.1	7.9	6.6	7.8	7.9
S_{slot} (mm^2)	330	586.9	585.1	401.2	578.7	637.4	333.5	575.9	521.8
w_2 (deg)	22.3	26.3	33.3	16.3	16.3	19.0	12.9	11.8	13.0
w_{2hal}	0.85	0.80	0.87	0.57	0.53	0.56	0.45	0.59	0.58

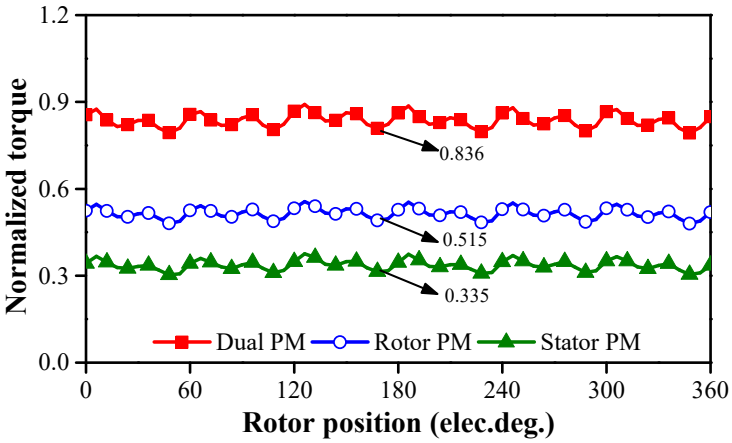

Figure 5. Torque decomposition of 12S11R1Pa SSDPM machine when relative permeability is 50.

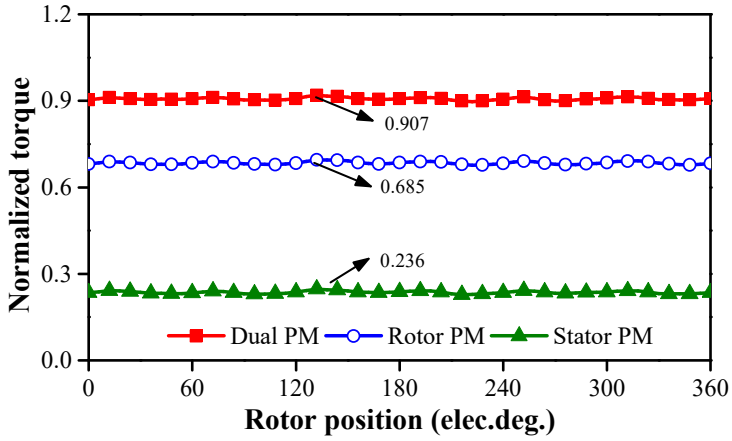

Figure 6. Torque decomposition of 12S23R1Pa STDPM machine when relative permeability is 50.

3. Influence of Rotor Slot Number

As shown in (1) and (2), when the stator slot number and armature pole pair number are fixed, the rotor slot number can be chosen as $N_s + P_a$ and $N_s - P_a$ for SSDPM machine, and $nN_s + P_a$ and $nN_s - P_a$ for STDPM machine. To compare the effect of rotor slot number selection, 12S1Pa SSDPM machines with 11R and 13R, 12S1Pa STDPM machine with 23R and 25R are investigated, respectively, as shown in Figures 7 and 8.

For fair comparison, all the investigated machine topologies are globally optimized for maximum torque under the same stator outer diameter, stack length, copper loss (120 °C) (copper loss is set according to the thermal restriction). All the optimizations are based on Genetic Algorithm (GA), and 30 individuals in each population with 35 generations have been employed. Tables 1 and 3 list the key design dimensions. In addition, the end winding length is calculated by the following equation:

$$l_{end} = y\pi^2(r_3 - y_k - 0.5s_h)/N_s, \quad (3)$$

in which y is the slot pitch, r_3 is the stator outer radius, y_k is the stator yoke width, s_h is slot height.

Figures 9 and 10 show that when the rotor slot number is selected lower than the stator slot number, higher torque can be produced. More importantly, higher power factor, lower iron loss, and higher efficiency can also be achieved with lower rotor slot number, as listed in Table 4, due to lower electrical frequency.

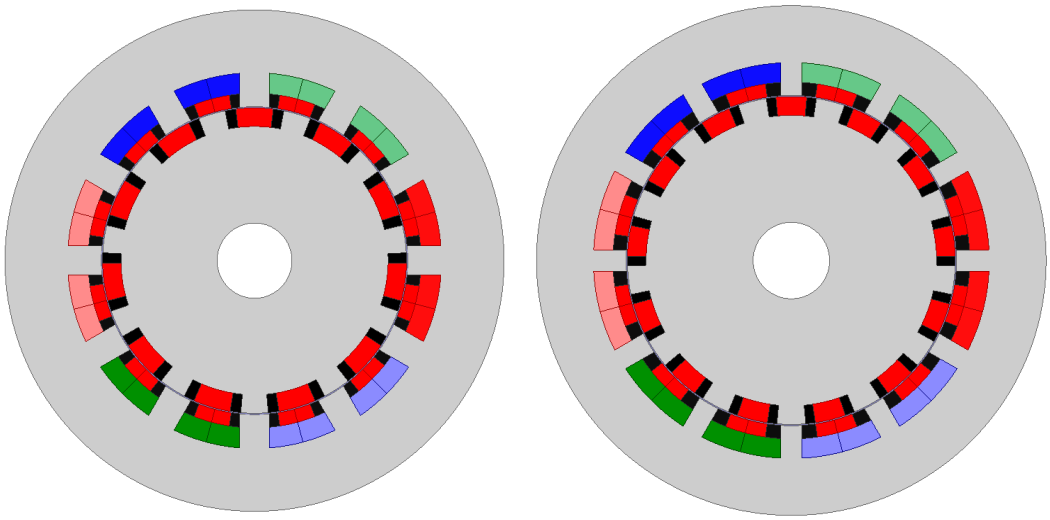

(**a**) 12S11R1Pa (**b**) 12S13R1Pa

Figure 7. Twelve-stator-slot SSDPM machines with a different rotor slot number. (**a**) 12S11R1Pa; (**b**) 12S13R1Pa.

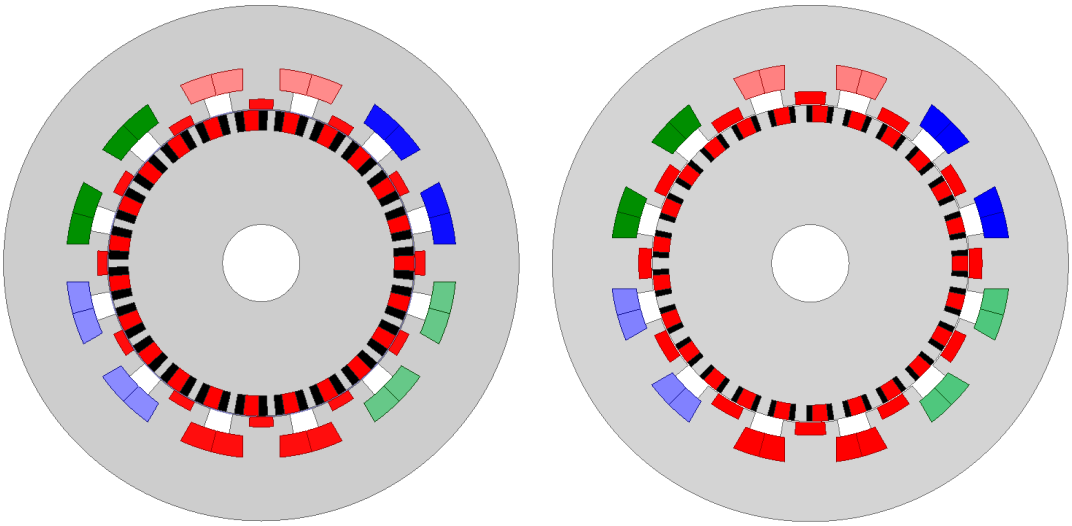

(**a**) (**b**)

Figure 8. Twelve-stator-slot STDPM machines with a different rotor slot number. (**a**) 12S23R1Pa; (**b**) 12S25R1Pa.

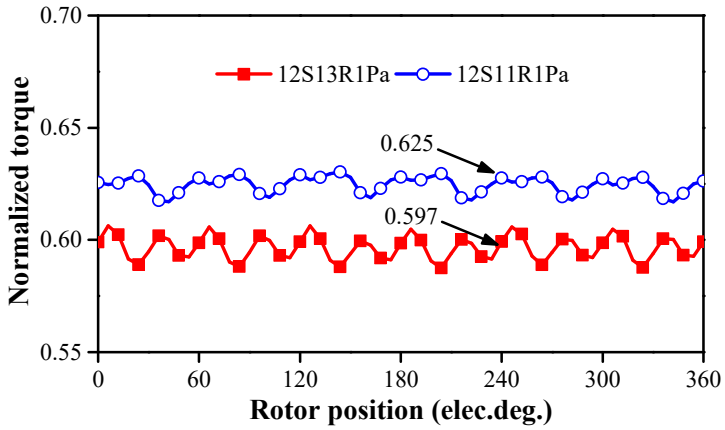

Figure 9. Torque waveforms of 12S1Pa SSDPM machines.

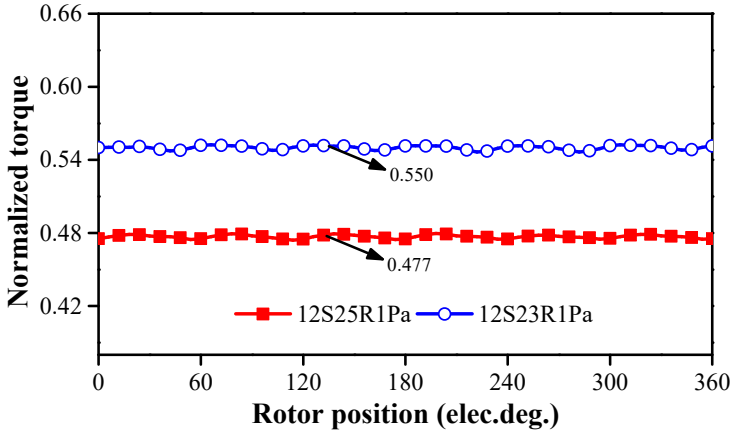

Figure 10. Torque waveforms of 12S1Pa STDPM machines.

Table 3. Parameters of optimized 12-slot STDPM machines with a different split-tooth number and armature pole pair number.

Symbol	2 Split-Tooth					3 Split-Tooth				4 Split-Tooth			
	12S23R1Pa	12S25R1Pa	12S22R2Pa	12S20R4Pa	12S19R5Pa	12S35R1Pa	12S34R2Pa	12S32R4Pa	12S31R5Pa	12S47R1Pa	12S46R2Pa	12S44R4Pa	12S43R5Pa
tw (mm)	14.6	19.9	18.6	22.2	23.0	6.7	21.7	22.1	22.4	11.7	16.1	21.8	15.8
w_1 (deg)	8.6	10.4	8.9	8.3	9.4	6.4	6.6	6.2	6.0	4.6	4.1	4.2	3.8
yk (mm)	24.3	22.6	16.1	12.4	12.0	24.7	17.4	10.2	11.1	24.4	18.9	12.2	8.6
h_t (mm)	7.6	6.5	7.5	8.1	6.8	6.5	7.6	6.9	5.9	6.1	5.8	6.6	5.4
so (deg)	8.6	10.4	8.9	8.3	9.4	6.4	6.6	6.2	6.0	4.6	4.1	4.2	3.8
r_1 (mm)	59.3	61.2	64.8	66.9	69.1	61.4	65.5	71.7	68.7	61.0	64.5	73.1	73.4
h_1 (mm)	3.8	4.9	4.6	4.5	4.1	4.6	4.2	3.0	3.0	4.9	2.60	3.6	3.2
h_2 (mm)	7.7	6.3	7.6	5.6	7.6	5.8	7.0	6.7	8.0	3.7	5.9	6.9	7.6
S_{slot} (mm^2)	190	168.2	248.2	246.2	231.3	210.9	173	235.6	281.8	205.8	242.3	167.8	351.4
w_2 (deg)	12.6	9.9	12.9	13.4	12.6	7.5	6.9	7.6	7.8	6.1	5.5	5.8	6.3
w_{2hal}	0.47	0.58	0.52	0.47	0.54	0.41	0.57	0.69	0.58	0.49	0.49	0.47	0.42

Table 4. Comparison of electromagnetic performances with a different rotor slot number selection under 600 rpm and the same copper loss.

	Normalized Torque (p.u.)	Normalized Power Factor (p.u.)	Normalized Iron Loss (p.u.)	Efficiency
12S11R1Pa SSDPM	0.625	0.547	0.36	83.0%
12S13R1Pa SSDPM	0.597	0.493	0.38	82.3%
12S23R1Pa STDPM	0.550	0.293	0.89	80.3%
12S25R1Pa STDPM	0.477	0.267	0.95	77.8%

4. Influence of Different Slot/Pole Number Combinations

Apart from the influence of stator yoke width, stator/rotor PM width, rotor diameter, stator/rotor PM height, for SSDPM machines with different slot/pole number combinations, the torques are mainly affected by pole ratio (pole ratio is an important index for flux modulation machines, and can be defined as N_r/P_a.) [33], flux leakage [33], end winding length, and winding factor. All the machine topologies are globally optimized for maximum torque under the aforementioned conditions, and the design details are all listed in Tables 1–3.

Figure 11 shows the influence of stator slot number and armature pole pair number on the average torques of SSDPM machines. The peak torques of 12S, 18S, 24S, 30S, and 36S appear when the armature pole pair numbers are 2, 3, 2, 2, and 4, respectively. On one hand, these combinations have shorter end winding length compared with those having 1 armature pole pair number. On the other hand, they have higher pole ratio than those

having larger armature pole pair number. The 12S7R5Pa SSDPM machine exhibits higher torque than the 12S8R4Pa one due to higher winding factor.

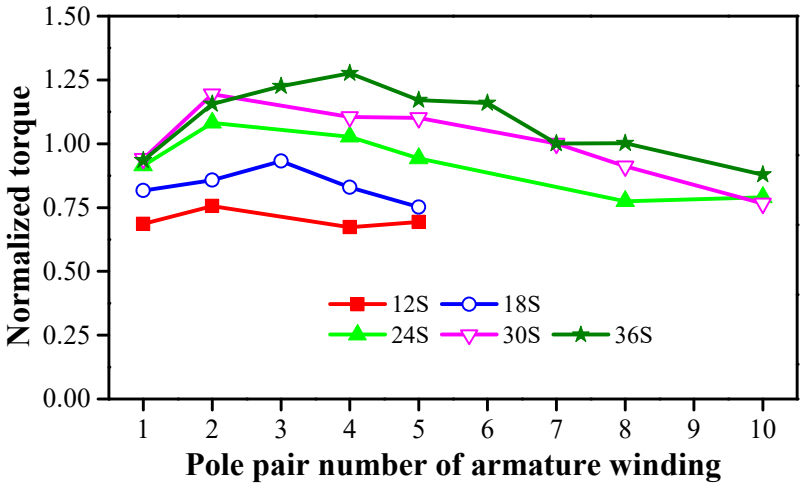

Figure 11. Torques versus armature pole pair number and stator slot number when rotor slot number is selected as $N_s - P_a$.

It should be noted that the maximum torque values also increase with the increase of stator slot number, as shown in Figure 12. Dual-PM machines with stator slot number larger than 36 are not calculated because:

(a) The increase of electrical frequency significantly affects other indexes, e.g., increasing the losses, decreasing the power factor, increasing the carrier frequency. All of these will deteriorate the overall performances. Figure 12 shows that the torque/electrical frequency decreases with the increase of stator slot number.

(b) The maximum torque increase rate decreases. When increasing the stator slot number from 12 to 18, the maximum torque increases by 0.176 p.u. However, when the stator slot number increases from 30 to 36, the maximum torque increases by 0.08 p.u. Hence, it is not cost-effective to further increase the stator slot number.

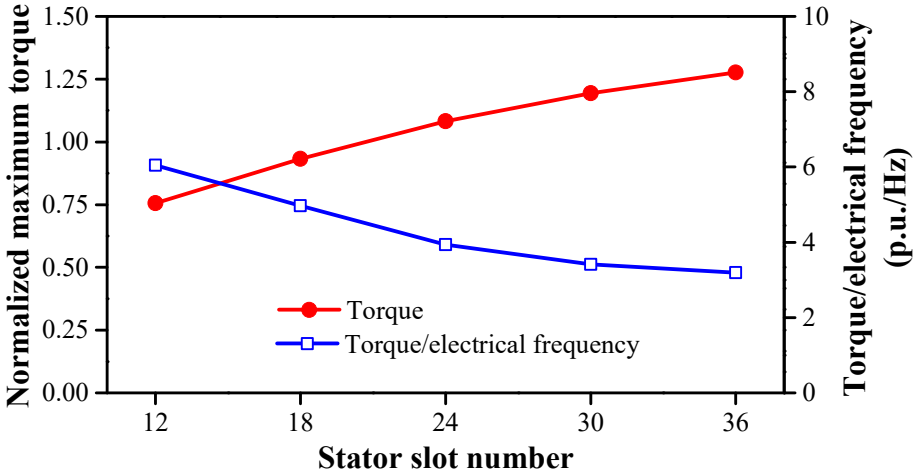

Figure 12. Maximum torque and torque/electrical frequency versus stator slot number at 600 rpm.

The torque ripples of SSDPM machines are shown in Figure 13. The 12S8R4Pa, 24S16R8Pa, and 30S20R10Pa exhibit significantly higher torque ripple than other combinations. This is due to the fact that these combinations have the smallest least common multiple (LCM) of the rotor slot number and the stator slot number.

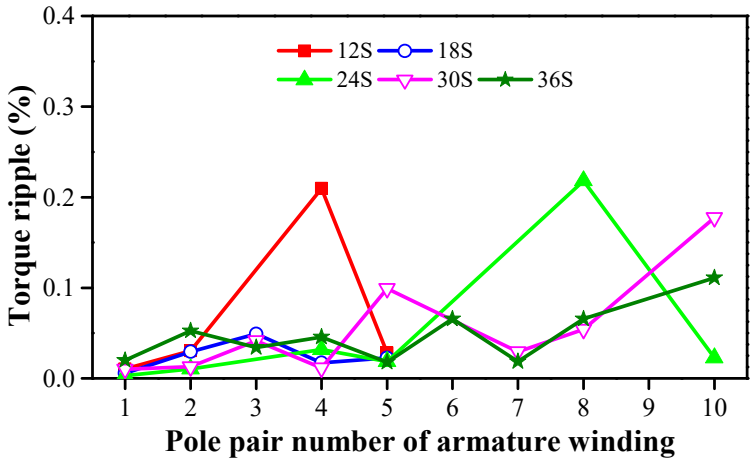

Figure 13. Torque ripples versus armature pole pair number and stator slot number when rotor slot number is selected as $N_s - P_a$.

Torques and torque ripples of STDPM machines are shown in Figures 14 and 15, respectively. Apart from the aforementioned influence factors, split-tooth number will increase the pole ratio, and thus affect the torque characteristics.

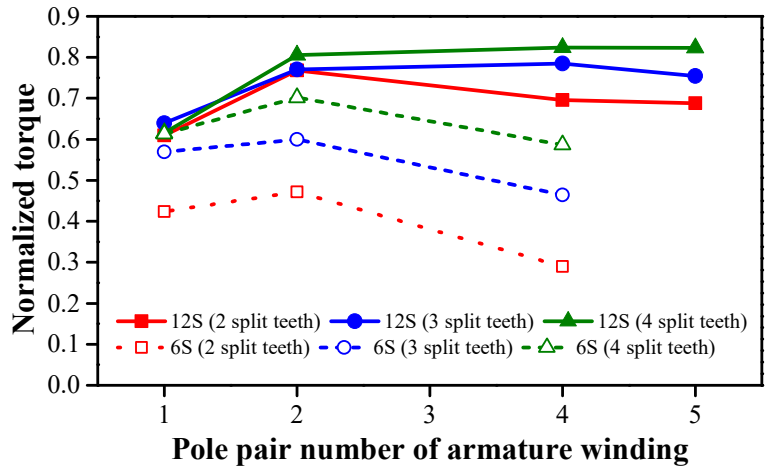

Figure 14. Torques versus stator slot number, armature pole pair number, and split-tooth number when rotor slot number is selected as $nN_s - P_a$.

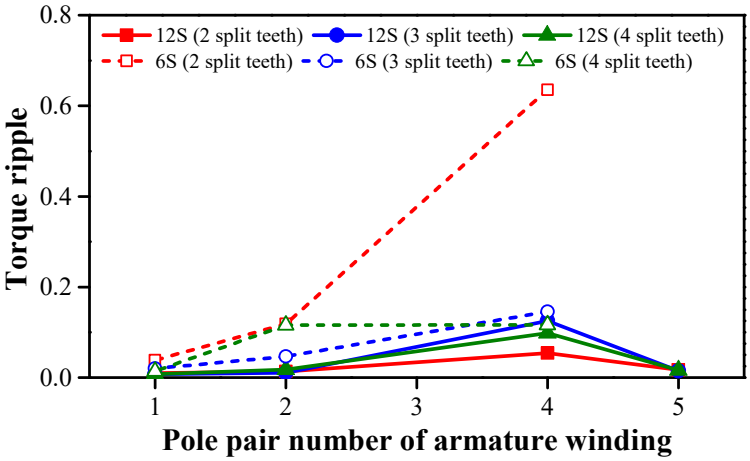

Figure 15. Torque ripples versus stator slot number, armature pole pair number, and split-tooth number when rotor slot number is selected as $nN_s - P_a$.

When the stator slot number is 6, increasing the split tooth number will increase the torque. However, when the stator slot number is 12 and the armature pole number is 1, increasing the split tooth number does not increase the torque, due to the increased flux leakage, as shown in Figure 16.

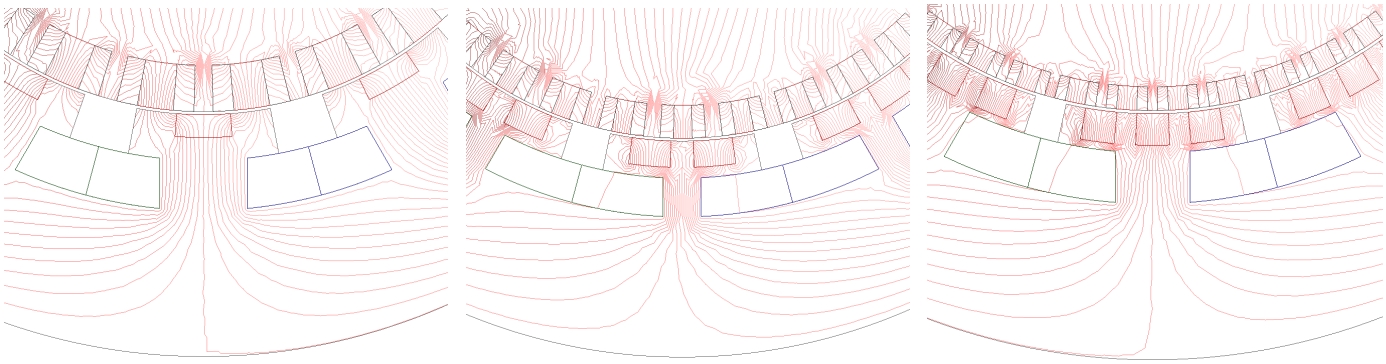

(a) (b) (c)

Figure 16. Flux line distributions of 12S1Pa STDPM machines with a different split tooth number at open-circuit condition. (**a**) 2 split teeth; (**b**) 3 split teeth; (**c**) 4 split teeth.

5. Comparison of Stator Slot Dual-PM Machine and Split Tooth Dual-PM Machine

In this section, the 24S20R4Pa SSDPM machine with distributed windings and the 12S20R4Pa STDPM machine with concentrated windings, as shown in Figure 17, are compared. Employing split-tooth mainly helps to ease manufacturing and decrease end winding length. These two combinations are chosen for comparison since they have the same armature pole pair number, rotor tooth number, pole ratio, stator outer diameter, and stack length. The design details of these two machines are listed in Tables 1 and 2.

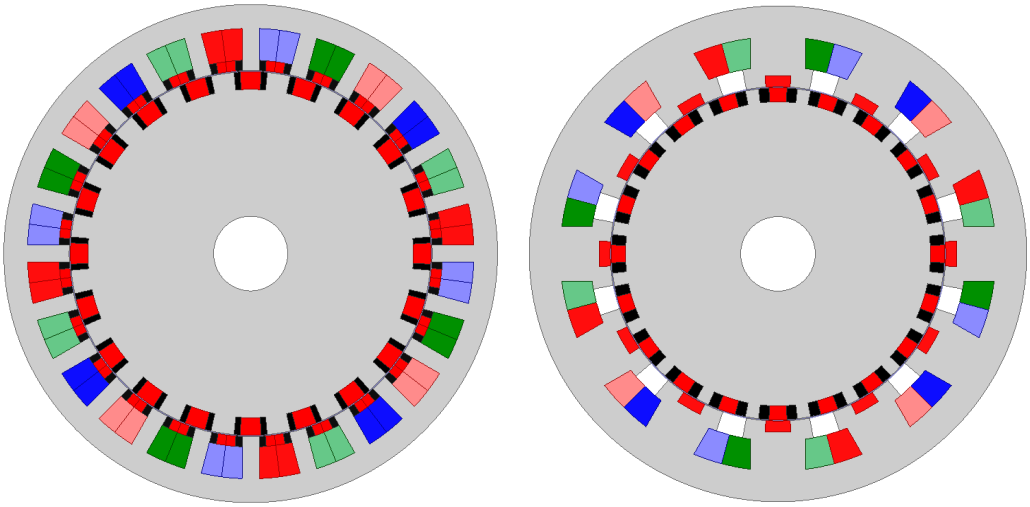

(a) (b)

Figure 17. Topologies of two dual-PM machines. (**a**) 24S20R4Pa SSDPM machine; (**b**) 12S20R4Pa STDPM machine.

Figure 18 compares the torque waveforms of the two machines under the same copper loss (120 °C). The SSDPM machine can deliver 48% higher torque with 63.2% lower torque ripple compared with the STDPM machine.

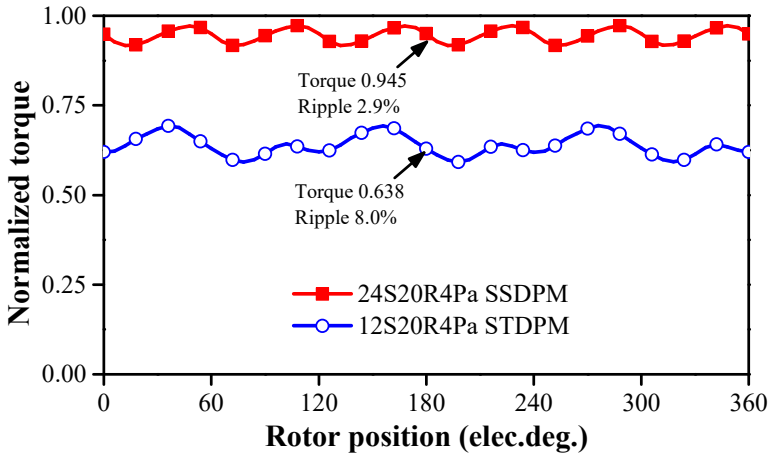

Figure 18. Comparison of torque waveforms of two dual-PM machines under the same copper loss (120 °C).

In actual operation, both DC voltage and phase current are limited. Here, space vector pulse width modulation (SVPWM) control strategy is employed. The turn number per slot is adjusted as 10. The parallel branch is adjusted to 2 and 1, for the SSDPM and STDPM machines, respectively.

Figure 19 shows the flux density distributions of the two compared dual-PM machines at open circuit condition and load condition ($I_d = 0$ and $I_q = I_{max}$). For the SSDPM and STDPM machines, the maximum flux density appears in the tooth and the split teeth, respectively, no matter what the condition is. In addition, slightly higher flux density can be observed in the yoke of the SSDPM machine at load condition. Despite this, the SSDPM exhibits better overload capability, which will be shown later. Hence, for both machines, the iron core material is fully utilized.

Figure 20 compares the back EMFs of the two dual-PM machines. The SSDPM machine exhibits 40.4% higher fundamental harmonic, albeit with much higher 5th harmonic. The STDPM machine has obvious 2nd harmonic due to unbalanced PM magnetomotive force (MMF).

Figure 21 shows the cogging torques of the two compared machines. The cogging torque of the STDPM machine is 3.6 times larger than the SSDPM machine, which explains the higher torque ripple in the STDPM machine. For the SSDPM and STDPM machines, the fluctuation frequency in one electrical period is 6 and 3, respectively. The higher amplitude and lower fluctuation frequency of the cogging torque of the STDPM machine are mainly due to its smaller least common multiple (LCM) of the stator slots and the rotor poles.

Figure 22 shows that the SSDPM machine produces 46% higher torque than the STDPM machine, together with 51.7% lower torque ripple. This is due to the fact that the rotor PM and stator PM in the SSDPM machine produce 26% and 122% higher torque than their counterparts, as shown in Figure 23. It can also be concluded that the stator PM machine with Halbach array PMs in the stator slots can deliver much higher torque than that with PMs between split teeth.

Figure 24 shows that the SSDPM machine has better overload capability than the STDPM machine. The overload capability can be indicated by inductance. The former has smaller inductance than the latter. This is due to the fact that the inductance is inversely proportional to the length of the flux path and the SSDPM has a longer flux path, as shown in Figure 19a,b. The torques/powers versus speed are calculated according to [33], and shown in Figure 25. The two dual-PM machines have similar corner speed. The SSDPM machine can produce 50.3% higher power than its counterpart.

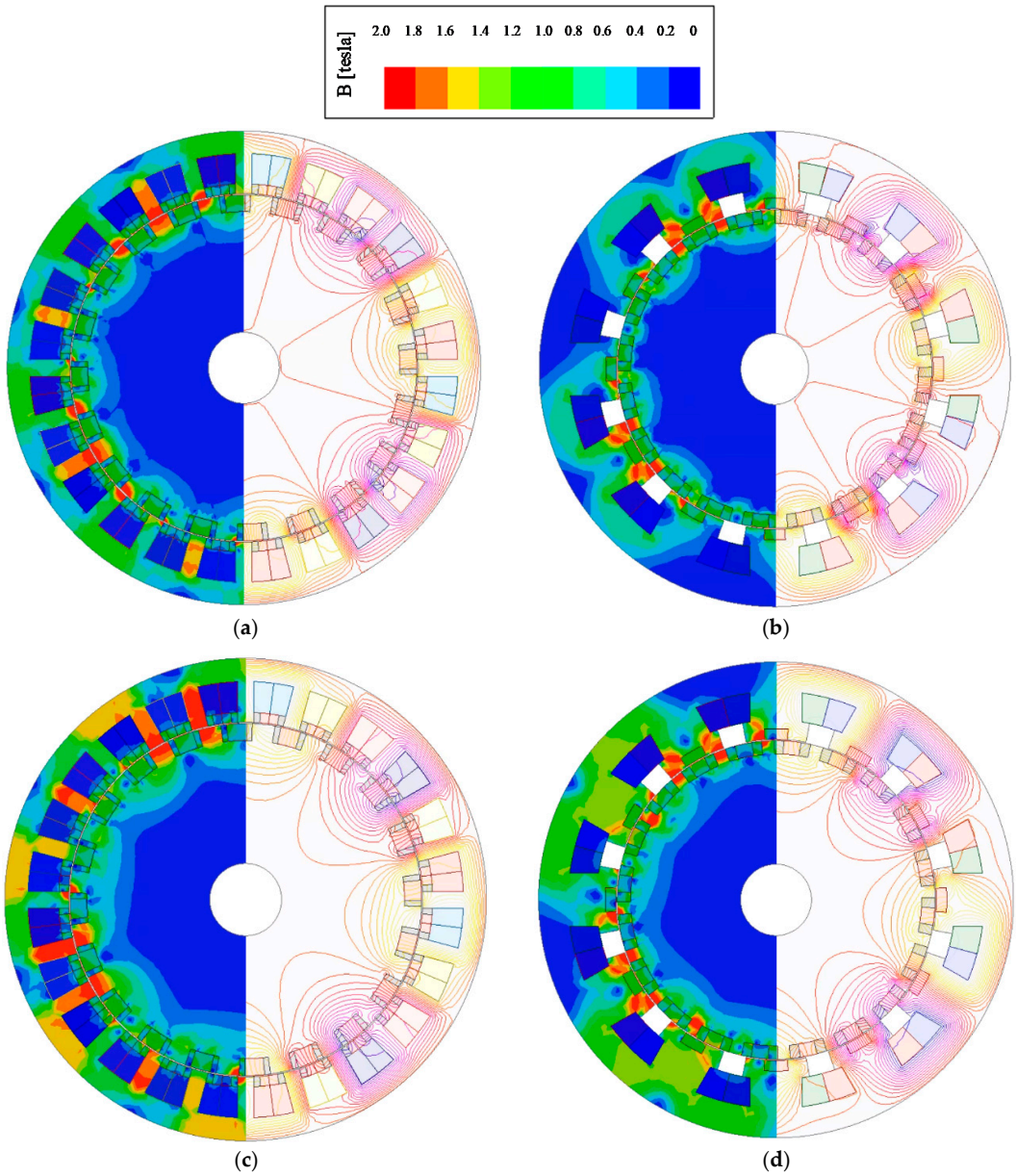

Figure 19. Flux density distributions of two dual-PM machines. (**a**) 24S20R4Pa SSDPM machine at open circuit condition; (**b**) 12S20R4Pa STDPM machine at open circuit condition; (**c**) 24S20R4Pa SSDPM machine at load condition (I_d = 0 and I_q = I_{max}); (**d**) 12S20R4Pa STDPM machine at load condition (I_d = 0 and I_q = I_{max}).

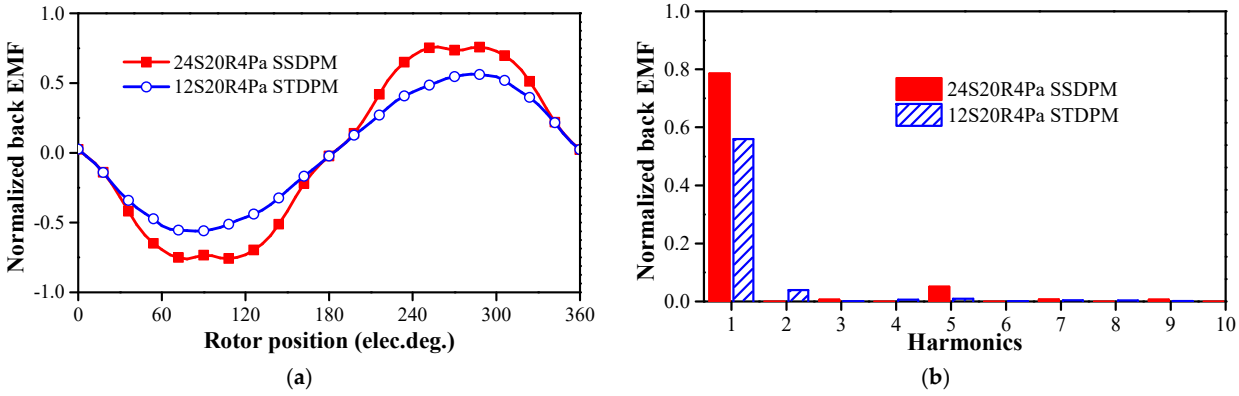

Figure 20. Back EMFs of two dual-PM machines at 600 rpm. (**a**) Waveforms; (**b**) spectra.

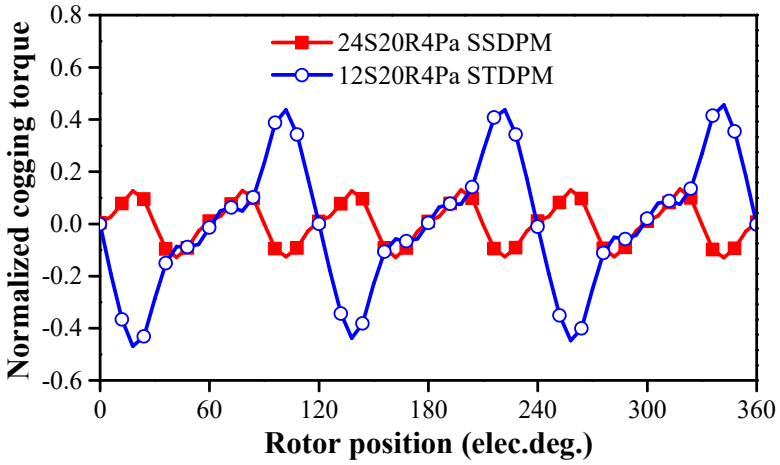

Figure 21. Cogging torques of two dual-PM machines.

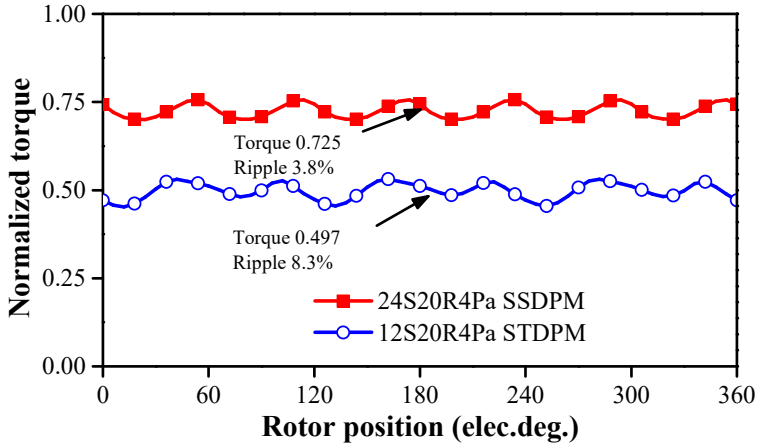

Figure 22. Torque waveforms of two dual-PM machines when $I = I_{max}$ and turn number per phase is adjusted to satisfy inverter requirements.

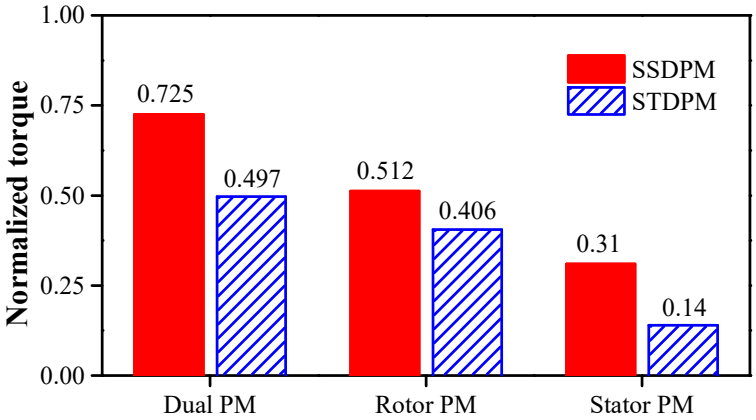

Figure 23. Torque decomposition of two dual-PM machines using frozen permeability method.

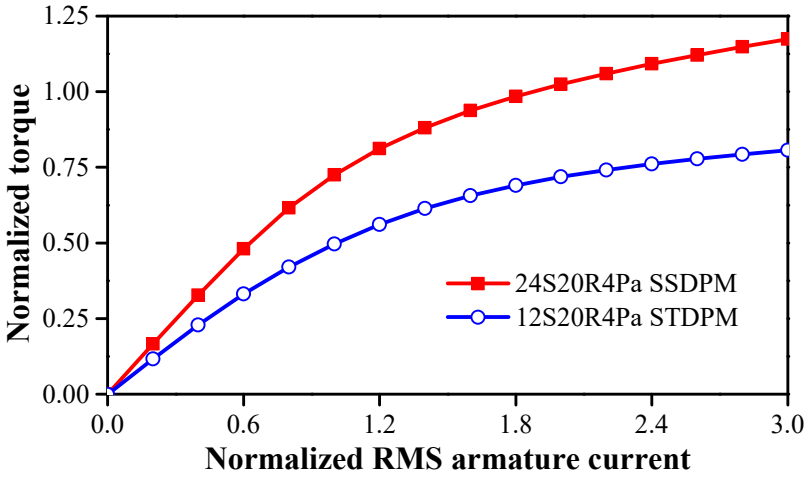

Figure 24. Torques versus current of two dual-PM machines.

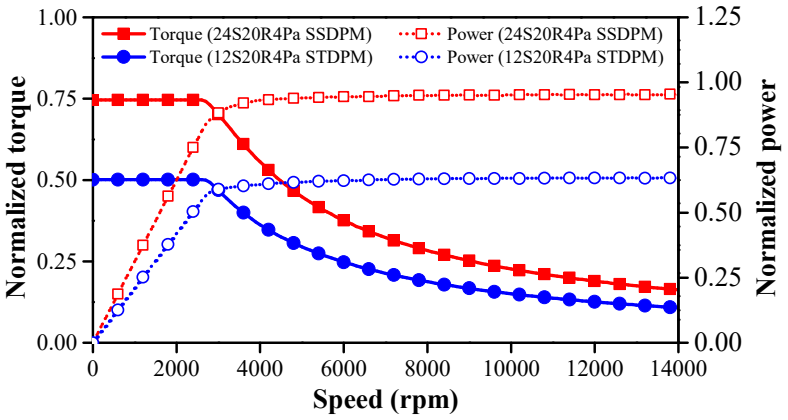

Figure 25. Torques/powers versus speed of two dual-PM machines.

Table 5 compares the electromagnetic performances of the dual-PM machines. The SSDPM machine has higher torque, higher torque per PM volume, higher power factor, and higher efficiency. Hence, the SSDPM machine is preferred.

Table 5. Comparison of electromagnetic performances of two dual-PM machines under 600 rpm and the same copper loss.

	24S20R4Pa SSDPM	12S20R4Pa STDPM
Normalized torque (p.u.)	0.725	0.497
Torque per PM volume (p.u./cm^3)	1.34	1.28
Normalized power factor (p.u.)	0.93	0.69
D-axis inductance (μH)	56.9	61.1
Q-axis inductance (μH)	62.59	61.4
Normalized iron loss (p.u.)	0.33	0.24
Efficiency	93.5%	89.7%

6. Conclusions

Two types of dual-PM machines, i.e., SSDPM machine and STDPM machine, are analyzed in terms of working principle, slot/pole number combinations, along with the comparison of electromagnetic performances. The results show that:

(a) Dual-PM machines can be decomposed into stator PM machines and rotor PM machines that share the same slot/pole number combinations.
(b) There exists one optimum armature pole pair number for maximum torque.
(c) The SSDPM machines exhibits better electromagnetic performances than the STDPM machines.

Author Contributions: The work presented in this paper is the output of an Innovate UK research project, HiTEV, jointly undertaken by The University of Sheffield and Nissan Technical Centre Europe. Z.Q.Z., D.A.S., M.P.F., and B.B. are the project investigators, while H.Q., J.R., T.M., D.I., T.K., K.S., and J.G., are the project team members, all contributed to the FEA calculation, analyses, discussions and the paper writing. All authors have read and agreed to the published version of the manuscript.

Funding: This research was funded by Innovate UK, grant number 105386.

Data Availability Statement: The data presented in this study are available on request from the corresponding author. The data are not publicly available due to confidentiality.

Conflicts of Interest: The authors declare no conflict of interest.

Abbreviations

μ_r	Relative permeability of PM material
B_r	Remanence of PM material
g	Airgap length
h_1	Stator PM height
h_2	Rotor PM height
h_t	Tooth tip height
l_{stk}	Stack length
r_1	Rotor outer radius
r_3	Stator outer radius
tw	Stator tooth width
S_{slot}	Slot area
w_1	Stator PM width
w_{1hal}	Width of radially magnetized PM in stator Halbach PM array
w_2	Rotor PM width
w_{2hal}	Width of radially magnetized PM in rotor Halbach PM array
yk	Stator yoke width
I_{max}	Amplitude of maximum current
I_d	D-axis current
I_q	Q-axis current

References

1. Atallah, K.; Rens, J.; Mezani, S.; Howe, D. A Novel "Pseudo" Direct-Drive Brushless Permanent Magnet Machine. *IEEE Trans. Magn.* **2008**, *44*, 4349–4352. [CrossRef]
2. Cooke, G.; Atallah, K. "Pseudo" Direct Drive Electrical Machines with Alternative Winding Configurations. *IEEE Trans. Magn.* **2017**, *53*, 1–8. [CrossRef]
3. Penzkofer, A.; Atallah, K. Analytical Modeling and Optimization of Pseudo-Direct Drive Permanent Magnet Machines for Large Wind Turbines. *IEEE Trans. Magn.* **2015**, *51*, 1–14. [CrossRef]
4. Li, D.; Qu, R.; Lipo, T.A. High-Power-Factor Vernier Permanent-Magnet Machines. *IEEE Trans. Ind. Appl.* **2014**, *50*, 3664–3674. [CrossRef]
5. Ishizaki, A.; Tanaka, T.; Takasaki, K.; Nishikata, S. Theory and optimum design of PM Vernier motor. In Proceedings of the International Conference on Electrical Machines and Drives, Durham, UK, 11–13 September 1995; pp. 208–212.
6. Wu, Z.Z.; Zhu, Z.Q. Analysis of Air-Gap Field Modulation and Magnetic Gearing Effects in Switched Flux Permanent Magnet Machines. *IEEE Trans. Magn.* **2015**, *51*, 1–12. [CrossRef]
7. Qu, R.; Li, D.; Wang, J. Relationship between magnetic gears and vernier machines. In Proceedings of the International Conference on Electrical Machines and Systems, Beijing, China, 20–23 August 2011; pp. 1–6.
8. Wu, Z.Z.; Zhu, Z.Q. Analysis of Magnetic Gearing Effect in Partitioned Stator Switched Flux PM Machines. *IEEE Trans. Energy Convers.* **2016**, *31*, 1239–1249. [CrossRef]

9. Chen, Y.; Fu, W.; Weng, X. A Concept of General Flux-Modulated Electric Machines Based on a Unified Theory and Its Application to Developing a Novel Doubly-Fed Dual-Stator Motor. *IEEE Trans. Ind. Electron.* **2017**, *64*, 9914–9923. [CrossRef]
10. Cheng, M.; Chau, K.; Chan, C. Static characteristics of a new doubly salient permanent magnet motor. *IEEE Trans. Energy Convers.* **2001**, *16*, 20–25. [CrossRef]
11. Chen, J.T.; Zhu, Z.Q. Winding Configurations and Optimal Stator and Rotor Pole Combination of Flux-Switching PM Brushless AC Machines. *IEEE Trans. Energy Convers.* **2010**, *25*, 293–302. [CrossRef]
12. Chen, J.T.; Zhu, Z.Q.; Iwasaki, S.; Deodhar, R. A novel E-core flux-switching PM brushless AC machine. In Proceedings of the IEEE Energy Conversion Congress & Expo, Atlanta, GA, USA, 12–16 September 2010; pp. 3811–3818.
13. Deodhar, R.; Andersson, S.B.; Boldea, I.; Miller, T. The flux-reversal machine: A new brushless doubly-salient permanent-magnet machine. *IEEE Trans. Ind. Appl.* **1997**, *33*, 925–934. [CrossRef]
14. Wang, C.; Nasar, S.A.; Boldea, I. Three-phase flux reversal machine (FRM). *IEEE Proc. Electr. Power Appl.* **1999**, *146*, 139. [CrossRef]
15. Li, J.; Chau, K.T.; Jiang, J.Z.; Liu, C.; Li, W. A New Efficient Permanent-Magnet Vernier Machine for Wind Power Generation. *IEEE Trans. Magn.* **2010**, *46*, 1475–1478. [CrossRef]
16. Kim, B.; Lipo, T.A. Operation and design principles of a PM vernier motor. *IEEE Trans. Ind. Appl.* **2014**, *50*, 3656–3663. [CrossRef]
17. Jang, D.K.; Chang, J.H. Design of a Vernier Machine with PM on Both Sides of Rotor and Stator. *IEEE Trans. Magn.* **2014**, *50*, 877–880. [CrossRef]
18. Wang, Q.; Niu, S.; Yang, L. Design Optimization and Comparative Study of Novel Dual-PM Excited Machines. *IEEE Trans. Ind. Electron.* **2017**, *64*, 9924–9933. [CrossRef]
19. Liu, Y.; Fu, W.N.; Guo, X.; Li, Z.; Fang, R. A dual permanent magnet machine for high-torque low-speed applications. In Proceedings of the 20th International Conference on Electrical Machines and Systems (ICEMS), Sydney, Australia, 11–14 August 2017; pp. 1–4.
20. Xie, K.; Li, D.; Qu, R.; Gao, Y. A Novel Permanent Magnet Vernier Machine with Halbach Array Magnets in Stator Slot Opening. *IEEE Trans. Magn.* **2017**, *53*, 1–5. [CrossRef]
21. Gao, Y.; Li, D.; Qu, R.; Ding, H. Synthesis of Novel Flux Modulation Machine with Permanent Magnets on Both Stator and Rotor. In Proceedings of the 2019 IEEE International Electric Machines & Drives Conference (IEMDC), San Diego, CA, USA, 12–15 May 2019; pp. 678–685.
22. Jia, S.; Qu, R.; Li, D.; Li, J. A High Torque Density Vernier PM Machines for Hybrid Electric Vehicle Applications. In Proceedings of the 2016 IEEE Vehicle Power and Propulsion Conference (VPPC), Hangzhou, China, 17–20 October 2016; pp. 1–6.
23. Zhu, Z.Q.; Hua, H.; Wu, D.; Shi, J.T.; Wu, Z.Z. Comparative Study of Partitioned Stator Machines with Different PM Excitation Stators. *IEEE Trans. Ind. Appl.* **2016**, *52*, 199–208. [CrossRef]
24. Wu, Z.Z.; Zhu, Z.Q. Partitioned Stator Flux Reversal Machine with Consequent-Pole PM Stator. *IEEE Trans. Energy Convers.* **2015**, *30*, 1472–1482. [CrossRef]
25. Wu, Z.Z.; Zhu, Z.Q.; Shi, J.T. Novel Doubly Salient Permanent Magnet Machines with Partitioned Stator and Iron Pieces Rotor. *IEEE Trans. Magn.* **2015**, *51*, 1–12. [CrossRef]
26. Evans, D.J.; Zhu, Z.Q. Novel Partitioned Stator Switched Flux Permanent Magnet Machines. *IEEE Trans. Magn.* **2014**, *51*, 1–14. [CrossRef]
27. Wang, F.; Zhou, L.; Wang, J.; Xiao, Y.; Zhou, J.; Shentu, L. A Novel Dual-Stator Permanent Magnet Vernier Machine with Magnets in Rotor and Both Stators. In Proceedings of the 21st International Conference on Electrical Machines and Systems (ICEMS), Jeju, Korea, 7–10 October 2018; pp. 197–201.
28. Wang, Q.; Niu, S. Design optimization and comparative analysis of dual-stator flux modulation machines. In Proceedings of the Annual Conference of the IEEE Industrial Electronics Society, Beijing, China, 5–8 November 2017; pp. 3719–3724.
29. Wang, H.; Fang, S.; Jahns, T.M.; Yang, H.; Lin, H. Design and Analysis of a Dual-Rotor Field Modulation Machine with Triple PM Excitation. In Proceedings of the 2018 IEEE Energy Conversion Congress and Exposition (ECCE), Portland, OR, USA, 23–27 September 2018; pp. 3302–3309.
30. Zhang, R.; Li, J.; Qu, R.; Li, D. A Novel Triple-Rotor Axial-Flux Vernier Permanent Magnet Machine. *IEEE Trans. Appl. Supercond.* **2016**, *26*, 1–5. [CrossRef]
31. Wu, L.; Qu, R.; Li, D.; Gao, Y. Influence of Pole Ratio and Winding Pole Numbers on Performance and Optimal Design Parameters of Surface Permanent-Magnet Vernier Machines. *IEEE Trans. Ind. Appl.* **2015**, *51*, 3707–3715. [CrossRef]
32. Ho, S.L.; Niu, S.; Fu, W.N. Design and Comparison of Vernier Permanent Magnet Machines. *IEEE Trans. Magn.* **2011**, *47*, 3280–3283. [CrossRef]
33. Chu, W.Q.; Zhu, Z.Q.; Zhang, J.; Liu, X.; Stone, D.A.; Foster, M.P. Investigation on Operational Envelops and Efficiency Maps of Electrically Excited Machines for Electrical Vehicle Applications. *IEEE Trans. Magn.* **2015**, *51*, 1–10. [CrossRef]